Радиофизика и радиоастрономия, 1997, т. 2, №3, 333-341
Radio Physics and Radio Astronomy, Kharkiv, IRA NASU Press, vol. 2, no 3, pp. 333-341, 1997

Numerical Analysis of Surface-Wave Filters Based on a Whispering-Gallery-Mode Dielectric Resonator and a Slitted Metal Cavity

Svetlana V. Boriskina and Alexander I. Nosich*

Radiophysics Department, Kharkov State University, Kharkov, 310077, Ukraine
**Institute of Radiophysics and Electronics National Academy of Sciences, Kharkov, 310085, Ukraine*

The paper is received by editor October 30, 1997

The scattering of a grounded dielectric layer surface wave from a circular dielectric cylinder and a slitted circular metallic cavity is analyzed in full-wave manner. By using the surface potential approach and analytical regularization, efficient numerical algorithms have been devised and applications to the bandstop filters are discussed. Computation results on the scattered, transmitted and reflected power fractions are presented, together with the near and far-field patterns in resonance points. The comparison of two types of filters is done.

1. Introduction

Localized discontinuities are known as important components of many optical and millimeter wave electronic systems that are based on the surface wave propagation. They are used as elements of integrated couplers, leaky-wave antennas, filters, resonators, etc. The design and manufacturing of such devices is a complicated technical task. To reduce their cost and improve the electromagnetic performance, a preceding CAD simulation, by using a reliable method and moderate computer hardware, is highly desirable. Simulations of relevant metal and dielectric discontinuities are frequently based on approximate theories [1]. Works [2,3] were devoted to the theoretical and experimental treatment of cylindrical dielectric resonators with whispering-gallery (WG) modes. A further theoretical and experimental work is necessary to optimize the performance of filters, couplers, and other passive devices. A more accurate analysis is especially important if studying the millimeter-wave applications, instead of optical ones, because here the device dimensions are comparable to the wavelength. However, it was only recently that adequate mathematical methods have been proposed, enabling one to attack the problem in correct full-wave manner [4-7]. However, they did not study specific applications such as filtering. This CAD-oriented analysis has been started in our recently published paper [8], for the circularly shaped dielectric and slitted-metal-cavity filters in the single-mode open waveguide. As such a simplified waveguide, we took an impedance plane in the H-polarization mode.

The purpose of the present study is to develop a method for modeling 2-D dielectric and metal scatterers in a more realistic multimode dielectric-slab waveguide. We wish to take account of the leaky and surface-wave effects, and compare different bandstop filters. To achieve the objectives, we use a combination of two methods. The first is the Green's function method which implies that the full Green's function (E or H-type) of a homogeneous dielectric slab is obtained analytically, and further used to derive the integral equation (IE) governing the field. Hence, satisfying the slab-interface continuity conditions is guaranteed, as well as the accounting of guided and leaky modes of the waveguide. The second is the family of techniques, which may be collectively named as the Method of Regularization (MoR) to treat the wave scattering problems, in mathematically accurate manner. It starts normally from a surface or volume IE well known in electromagnetics. However, unlike the Method of Moments (MoM), here it is partially inverted analytically, that results in the infinite matrix equation of the Fredholm 2-nd kind, thus giving a proof of existence of unique solution. This procedure is equivalent to a judicious choice of basis/testing functions in MoM, so that they form a set of orthogonal eigenfunctions of the inverted part of IE. Numerical solution of such matrix equation is always stable and efficient in terms of memory and CPU time expenses. To study the localized dielectric discontinuities, it is supposed to use the surface potential method, extracting out and analytically inverting the free-space-circular-cylinder part of the IE. To analyze metallic slitted-cavity scatterer, the static part of the electric field IE is to be inverted.

We considered both polarizations for the scattering from a dielectric resonator and the case of H-polarization for the cavity resonator. This is because the WG mode resonances are present in each polarization for the former, but it is only the H-case for the latter, when the low-frequency (the Helmholtz, or slot-mode) resonance exists, which is promising for filter applications (see [7]). All field quantities are assumed to have time variation $e^{-i\omega t}$ and this time factor is omitted throughout of the analysis.

© Svetlana V. Boriskina and Alexander I. Nosich, 1997

2. Method of analysis

2.1. Cylindrical dielectric resonator. The case of *H*-polarization

Consider the 2-D scattering problem depicted in Fig. 1a. An H-polarized guided mode of the grounded dielectric layer is incident from the left on a circular dielectric cylinder, whose dielectric constant is ε_b and radius a. The layer thickness is d and the dielectric constant is ε_s, while the separation from the cylinder is w. The magnetic field component of any surface-wave guided mode is known to be as follows:

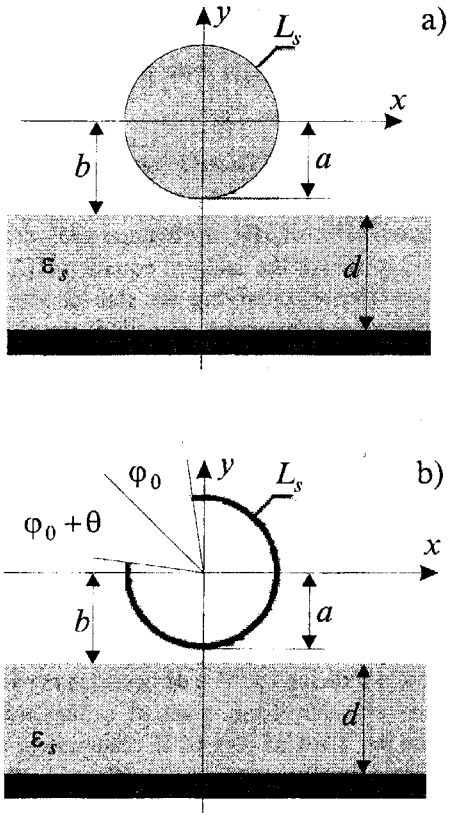

Fig. 1. *Geometry of the scattering problem*

$$H_z = V_n^H(y)\cdot e^{\pm ikh_n x} = e^{\pm ikh_n x}\times$$
$$\times\begin{cases}\cos(k\gamma_n(y+b+d)), & -d-b\le y\le -b,\\ \cos(k\gamma_n d)e^{-k\rho_n(y+b)}, & -b<y<\infty,\end{cases} \qquad (1)$$
$$n=0,1,\dots,N,$$

where $\pm$ denotes right/left moving waves, $b=w+a$, $\rho_n=\sqrt{h_n^2-1}$, $\gamma_n=\sqrt{\varepsilon_s-h_n^2}$, h_n: $1<h_n<\sqrt{\varepsilon}$ being the propagation constant of the n-th mode (n=0,1,...,N), and so a real root of the dispersion equation:

$$\mathrm{tg}(k\gamma_n d)=\varepsilon_s\rho_n\gamma_n^{-1}.$$

Functions (2) are normalized by using the following relation:

$$N_n^2=\int_{-(b+d)}^{\infty}\frac{1}{\varepsilon(y)}\left[V_n^H(y)\right]^2dy=$$
$$=\frac{d}{2\varepsilon_s}+\frac{1}{2k\rho_n}\cdot\frac{\gamma_n^2+\rho_n^2}{\gamma_n^2+\varepsilon_s^2\rho_n^2}$$

that yields the power carried by the n-th surface-wave mode.

The total magnetic field in such geometry consists of the incident H^{in} and scattered H^{sc} components, and the field inside the dielectric body is denoted as H^b. The total field satisfies the Helmholtz equation

$$\left[\Delta+k^2\varepsilon(\vec r)\right]H(\vec r)=0,$$
$$\vec r=(r,\varphi)\in D\setminus L_s,\quad D=(x,y), \qquad (2)$$

the boundary conditions on the contour L_s of the scatterer

$$H^{sc}+H^{in}=H^b,$$
$$\frac{1}{\varepsilon_b}\frac{\partial H^b}{\partial n}=\frac{\partial H^{sc}}{\partial n}+\frac{\partial H^{in}}{\partial n},\quad \vec r\in L_s, \qquad (3)$$

and on the waveguide boundaries (square brackets are for the jumps of functions):

$$\left[\frac{1}{\varepsilon(y)}\frac{\partial H}{\partial y}\right]=[H]=0,\quad y=-b,$$
$$\frac{\partial H}{\partial y}=0,\quad y=-(b+d), \qquad (4)$$

and a modified radiation condition that is, according to [9]:

$$H^{cs}(\vec r)\underset{r\to\infty}{\approx}\Phi^H(\varphi)\left(\frac{2}{i\pi kr}\right)^{1/2}e^{ikr}+$$
$$+\sum_{n=o}^{N}\begin{Bmatrix}T_n-\delta_{no}, & x>0\\ R_n, & x<0\end{Bmatrix}\cdot V_n^{(H)}(y)\cdot e^{ih_n|x|}. \qquad (5)$$

Representing the scattered field outside and inside the dielectric resonator in terms of the single-layer surface potentials,

$$H^b(\vec r)=\int_{L_s}\varphi^H(\vec r_s)G_b^H(\vec r,\vec r_s)dl_s, \qquad (6a)$$

(*) see a critical comment below

$$H^{sc}(\vec r)=\int_{L_s}\psi^H(\vec r_s)G^H(\vec r,\vec r_s)dl_s, \qquad (6b)$$

we obtain a pair of coupled IE with respect to the unknown density functions:

$$\int_{L_s}\varphi^H(\vec{r}_s)G_b^H(\vec{r},\vec{r}_s)dl_s -$$

$$-\int_{L_s}\psi^H(\vec{r}_s)G^H(\vec{r},\vec{r}_s)dl_s = H^{in}(\vec{r}),\ \ \vec{r}\in L_s, \tag{7a}$$

$$\frac{1}{\varepsilon_b}\frac{\partial}{\partial n}\int_{L_s}\varphi^H(\vec{r}_s)G_b^H(\vec{r},\vec{r}_s)dl_s -$$

$$-\frac{\partial}{\partial n}\int_{L_s}\psi^H(\vec{r}_s)G^H(\vec{r},\vec{r}_s)dl_s =$$

$$=\frac{\partial}{\partial n}H^{in}(\vec{r}),\ \ \vec{r}\in L_s. \tag{7b}$$

Here G_b^H is the Green's function of the homogeneous medium with permittivity ε_b, and G^H is the Green's function of the halfspace with a grounded dielectric slab, i.e.

$$G_b^H(\vec{r},\vec{r}_s)=\frac{i\varepsilon_b}{4}H_o^{(1)}(k\sqrt{\varepsilon_b}|\vec{r}-\vec{r}_s|),$$

$$G^H(\vec{r},\vec{r}_s)=\frac{i}{4}H_o^{(1)}(k|\vec{r}-\vec{r}_s|)+\frac{i}{4\pi}\times$$

$$\times\int_{-\infty}^{\infty}\frac{1}{g}\cdot\frac{ig\varepsilon_s\cos(k\gamma d)-\gamma\sin(k\gamma d)}{ig\varepsilon_s\cos(k\gamma d)+\gamma\sin(k\gamma d)}\times$$

$$\times e^{ikg(y+y_s+2b)+ikh(x-x_s)}dh,$$

where $g=\sqrt{1-h^2}$, $\gamma=\sqrt{\varepsilon_s-h^2}$. Then due to the geometry of the scatterer these IE can be reduced to a matrix equation by expanding the densities and the Green's functions in terms of angular exponents $\{e^{in\varphi}\}_{n=-\infty}^{\infty}$. In fact, here we use the fact that these functions form the set of orthogonal eigenfunctions of any integral operator in (7a) and (7b), if G^H has been replaced by its first term. That is why the final result is the regularized matrix equation:

$$\psi_m^H+\frac{i^m}{J_m(ka)(1+iB_m^H)}\times$$

$$\times\sum_{n=-\infty}^{\infty}\psi_n^H(-i)^nJ_n(ka)\Omega_{m+n}^H=$$

$$=-\frac{i^m(h_o+\rho_o)^m\cos(k\gamma_o d)}{J_m(ka)(1+iB_m^H)}e^{-\rho_o kb}, \tag{8}$$

where

$$\Omega_n^H=-H_n^{(1)}(2kb)+\frac{2i\varepsilon_s}{\pi}\times$$

$$\times\int_{-\infty}^{\infty}\frac{\cos(k\gamma d)(h-ig)^n}{ig\varepsilon_s\cos(k\gamma d)+\gamma\sin(k\gamma d)}e^{2ikgb}dh, \tag{9}$$

$$B_m^H=\frac{J_m'(k\sqrt{\varepsilon_b}a)Y_m(ka)-\sqrt{\varepsilon_b}J_m(k\sqrt{\varepsilon_b}a)Y_m'(ka)}{J_m'(k\sqrt{\varepsilon_b}a)J_m(ka)-\sqrt{\varepsilon_b}J_m(k\sqrt{\varepsilon_b}a)J_m'(ka)}.$$

The proof of the Fredholm 2-nd kind nature of (8) can be found in [4]. Due to this fact, it can be solved numerically, with a guaranteed convergence to the exact values of unknowns provided that the number of equations is taken greater. The expansion coefficients of the field inside the dielectric cylinder can be obtained via the following relation:

$$\varphi_n^H=\frac{J_n(ka)}{\varepsilon_b H_n^{(1)}(k\sqrt{\varepsilon_b}a)J_n(k\sqrt{\varepsilon_b}a)}\times$$

$$\times\Big[\psi_n^H H_n^{(1)}(ka)+i^n(h_o+\rho_o)^n\cos(k\gamma_o d)e^{-\rho_o kb}+$$

$$+i^n\sum_{m=-\infty}^{\infty}\psi_m^H(-i)^mJ_m(ka)\Omega_{m+n}\Big].$$

2.2. Cylindrical dielectric resonator. The case of *E*-polarization

The natural modes of the grounded dielectric waveguide in the E-polarization can be represented like follows:

$$E_z=V_n^E(y)\cdot e^{\pm ikh_n x}=e^{\pm ikh_n x}\times$$

$$\times\begin{cases}\sin(k\gamma_n(y+b+d)), & -d-b\le y\le -b,\\ \sin(k\gamma_n d)e^{-k\rho_n(y+b)}, & -b<y<\infty,\end{cases}$$

$n=1,2,\ldots,N.$

Unlike the H-polarization case, every E-polarized mode of a grounded dielectric slab has a finite cut-off frequency. Its wavenumber is a real root of the dispersion equation

$$\mathrm{tg}(k\gamma_n d)=-\gamma_n\rho_n^{-1},$$

and the norm of the mode is given by

$$N_n^2(y)=\int_{-(b+d)}^{\infty}\left[V_n^E(y)\right]^2dy=\frac{d}{2}+\frac{1}{2k\rho_n}.$$

By following the procedure described in the previous subsection we come to the resulting matrix equation:

$$\psi_m^E + \frac{i^m}{J_m(ka)(1+iB_m^E)} \times$$

$$\times \sum_{n=-\infty}^{\infty} \psi_n^E (-i)^n J_n(ka) \Omega_{m+n}^E =$$

$$= -\frac{i^m (h_1 + \rho_1)^m \sin(k\gamma_1 d)}{J_m(ka)(1+iB_m^E)} e^{-\rho_1 kb}, \qquad (10)$$

where

$$\Omega_n^E = -H_n^{(1)}(2kb) + \frac{2i}{\pi} \times$$

$$\times \int_{-\infty}^{\infty} \frac{\sin(k\gamma d)(h-ig)^n}{ig\sin(k\gamma d) - \gamma \cos(k\gamma d)} e^{2ikgb} dh, \qquad (11)$$

$$B_m^E = \frac{\sqrt{\varepsilon_b} J_m'(k\sqrt{\varepsilon_b}a) Y_m(ka) - J_m(k\sqrt{\varepsilon_b}a) Y_m'(ka)}{\sqrt{\varepsilon_b} J_m'(k\sqrt{\varepsilon_b}a) J_m(ka) - J_m(k\sqrt{\varepsilon_b}a) J_m'(ka)}.$$

To compute the functions $\Omega_n^{H(E)}$ one has to perform a numerical integration. As the integrands are not single-valued functions of h, we have two branch cuts arising from points ± 1 in the complex h-plane. Besides, there are the surface-wave poles at $h = \pm h_n$ on the real axis, plus the leaky-wave poles off it in the 1-st and the 3-rd quater-planes. Numerical evaluation of these integrals is one of the most time-consuming parts of the algorithm. To speed up the computation we follow the procedure proposed in [10]. First, we convert the integrals in (9) and (11) to the ones along the positive real semi-axis. Then the path of integration is deformed to the one composed of the four straight-line sections between the following points: 1) h=0, 2) h=-iT_a, 3) h=T_b-iT_a, 4) h=T_b, 5) h=T_c, where T_a=1, $T_b = \sqrt{\varepsilon_s} + 1$. The value of T_c depends on the rate of the integrand decay. Thus the integration around the poles is omitted and the infinite path of integration can be truncated because the integrand is decaying exponentially on the last segment.

2.3. Slitted circular-cavity resonator

The scattering geometry for this case is shown in Fig. 1b. Let us now represent the scattered field in the form of a double-layer potential:

$$H^{sc}(\vec{r}) = \int_{L_s} \mu(\vec{r}_s) \frac{\partial}{\partial n} G^H(\vec{r}, \vec{r}_s) dl_s. \qquad (12)$$

As in the previous subsection, this function should satisfy (2), (4) and (5), but on the contour of the scatterer the following condition is valid:

$$\frac{\partial H}{\partial n} = 0, \qquad \vec{r} \in L_s,$$

L_s being now a circular arc of the radius a. By following the procedure described in [6,7], we obtain a singular IE for the surface current density as:

$$\frac{\partial}{\partial n} \int_{L_s} \mu(\vec{r}_s) \frac{\partial}{\partial n_s} G^H(\vec{r}, \vec{r}_s) dl_s =$$

$$= -\frac{\partial}{\partial n} H^{in}(\vec{r}), \quad \vec{r} \in L_s. \qquad (13)$$

Equations of this type are often encountered in scattering problems. They can be solved numerically by direct applying the MoM. However, the solution scheme based on the analytical inversion of the static part of (13) is much more efficient. The current density function should be completed with identical zero on the slot. Retracing all the relevant steps from [7], we come to the dual series equations for the expansion coefficients. Further we regularize them by inverting the static part analytically and arrive at the following Fredholm 2-nd kind matrix equation:

$$\mu_m = \sum_{n=-\infty}^{\infty} \left[\Delta_n T_{mn} + i\pi (ka)^2 (-i)^n J_n'(ka) \times \right.$$

$$\left. \times \sum_{p=-\infty}^{\infty} i^p J_p'(ka) \Omega_{n+p}^H T_{mp} \right] \mu_n + i\pi (ka)^2 \times$$

$$\times \sum_{n=-\infty}^{\infty} T_{mn} i^n J_n'(ka)(h_o + \rho_o)^n \times \cos(k\gamma_0 d) e^{-\rho_o kb},$$

$$m = 0, \pm 1, \ldots,$$

where the coefficients T_{mn} are the functions of φ_o and θ and can be found in [6,7]. They are easily computed as combinations of exponents and the Legendre polynomials.

2.4. Far-field characteristics and procedure validation

To obtain the amplitudes of the guided mode at $x \to \pm\infty$ along the interface, one has to use the contour deformation in the complex h-plane and take account of the residues at the poles h=$\pm h_n$. For the dielectric resonator in the case of H-polarization:

$$\begin{Bmatrix} T_n^H - \delta_{no} \\ R_n^H \end{Bmatrix} = \frac{2}{h_n k N_n^2} \cos(k\gamma_n d) e^{-\rho_n kb} \times$$

$$\times \sum_{m=0}^{\infty} \psi_m^H (\mp i)^m J_m(ka)(h_n \pm \rho_n)^m. \qquad (14)$$

For the case of E-polarization cos (.) should be replaced by sin (.), and ψ_m^H by ψ_m^E. The far-field scattering patterns can be evaluated by applying the steepest-

descent method in the far zone of the scatterer. For the dielectric resonator:

$$\Phi^{H(E)}(\varphi) = \sum_{m=-\infty}^{\infty} \psi_m^{H(E)} (-i)^m J_m(ka) \times$$
$$\times \left(e^{im\varphi} + R^{H(E)}(\varphi) \cdot e^{2ikb\sin\varphi - im\varphi} \right), \qquad (15)$$
$$R^H(\varphi) = \frac{i\varepsilon_s \sin\varphi\cos(k\gamma d) - \gamma\sin(k\gamma d)}{i\varepsilon_s \sin\varphi\cos(k\gamma d) + \gamma\sin(k\gamma d)},$$
$$R^E(\varphi) = \frac{i\sin\varphi\sin(k\gamma d) + \gamma\cos(k\gamma d)}{i\sin\varphi\sin(k\gamma d) - \gamma\cos(k\gamma d)},$$
$$\gamma(\varphi) = \sqrt{\varepsilon_s - \cos^2\varphi}.$$

For the cavity resonator, (14) and (15) are still valid after replacing $\psi_m^H J_n(ka)$ by $\mu_m^H J_n'(ka)$.

The optical theorem, based on the energy conservation principle, serves as an independent partial check of the numerical code [9,11]. After validation, the theorem can be used to minimize the time needed to compute the total radiated power, as

$$P_{sc} \equiv \frac{2}{\pi} \int_o^{\pi} |\Phi(\varphi)|^2 d\varphi = kh_{inc} N_{inc}^2 -$$
$$\sum_{n=o(1)}^{N} kh_n N_n^2 \left\{ |T_n|^2 + |R_n|^2 \right\},$$

where h_{inc} and N_{inc}^2 are the wavenumber and the norm of the incident mode, respectively.

For the case of a non-symmetric scatterer such as cavity, the reciprocity theorem yields that the transmission of the incident guided mode is invariant of the direction of incidence:

$$T_{inc}(\varphi_o) = T_{inc}(\pi - \varphi_o)$$

(see [9] for a discussion of this phenomena).

To have a 3-digit accuracy in practical computations, it is enough to take the matrix truncation numbers as $N_{diel} = ka\sqrt{\varepsilon_b} + 3$ and $N_{cav} = ka + 10$, respectively. The truncation error is defined like follows: $\delta_N = \max\left|\psi(\mu)_n^{N+1} - \psi(\mu)_n^N\right| / \max\left|\psi(\mu)_n^N\right|$. As for the optical theorem and the reciprocity, they were satisfied with a 10^{-14} accuracy for all the values of the problem parameters. CPU time varies depending on the size of the scatterer. For example, computing a dielectric cylinder of ka=2, ε_b=10, with the PC Pentium, 100 MHz and the MS-DOS Fortran source code at double precision took 3 sec. For a cavity of ka=2 it took 2 sec.

3. Numerical results and discussion

Consider first a dielectric resonator. In Fig. 2, the plots of the far-field characteristics are shown as a function of the normalized frequency parameter ka for the H polarization. One can see that a dielectric cylinder can be used as a bandstop filter. The principle of operation of such a filter is based on the excitation of a WG mode in the resonator. In this case the field inside the dielectric cylinder is oscillating between the resonator boundary and an inner caustic. When the resonator is coupled to a waveguide, the resonances at the WG modes cause the resonances in the transmission coefficients of the guided modes. In many practical applications it is desired to have a single mode operation. A grounded dielectric slab supports, in the H-polarization, a single mode provided that $kd\sqrt{\varepsilon_s - 1} < \pi$. This mode is called the principal one, as it does not have a low-frequency cutoff.

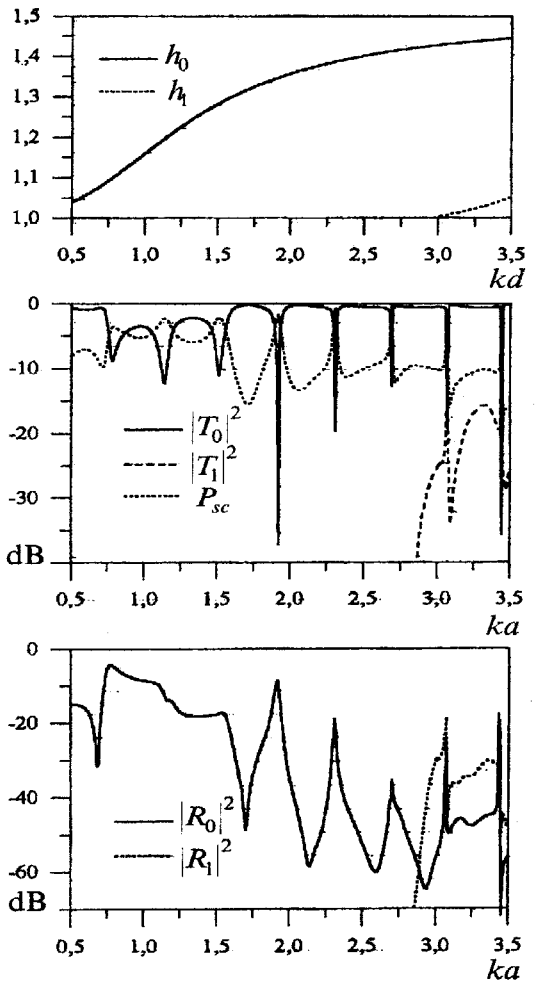

Fig. 2. *Far-field scattering characteristics versus ka for the dielectric resonator (H-polarization case).* ε_b=10, *w/a=0.01, d/a=1,* ε_s=2.25

For the case of E polarization filter characteristics versus ka are depicted in Fig. 4. In this case there is no principal mode, all the modes have cutoff frequencies.

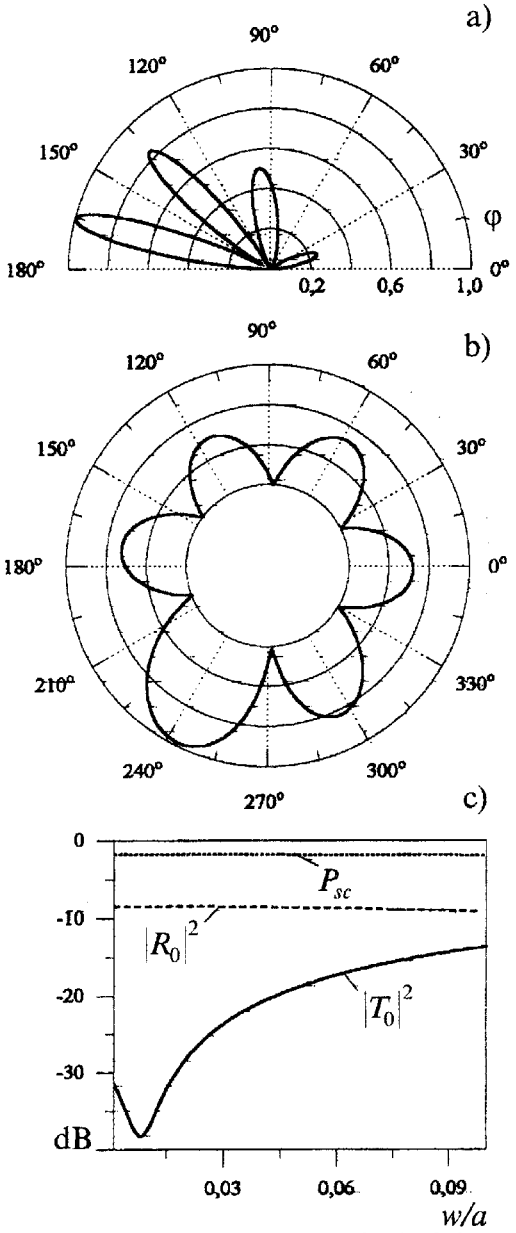

Fig. 3. *a) Normalized scattering pattern for the dielectric resonator (H-polarization case).* ε_b*=10, w/a=0.01, d/a=1,* ε_s*=2.25, ka=1.9168*
b) Magnetic field distribution on the contour of the resonator with the same parameters
c) Filter characteristics versus the spacing between the resonator and the waveguide

Figures 3 and 5b show the field variations on the contour of the dielectric resonator. By the number of lobes in this plot and their location with respect to the symmetry axis the WG resonances can be classified. Due to the symmetry of the problem geometry, the coincidence of the resonant frequencies of different modes may occur. A possible way to avoid this difficulty is to disturb the symmetry of the problem, for example, to use a non-uniform dielectric resonator [3].

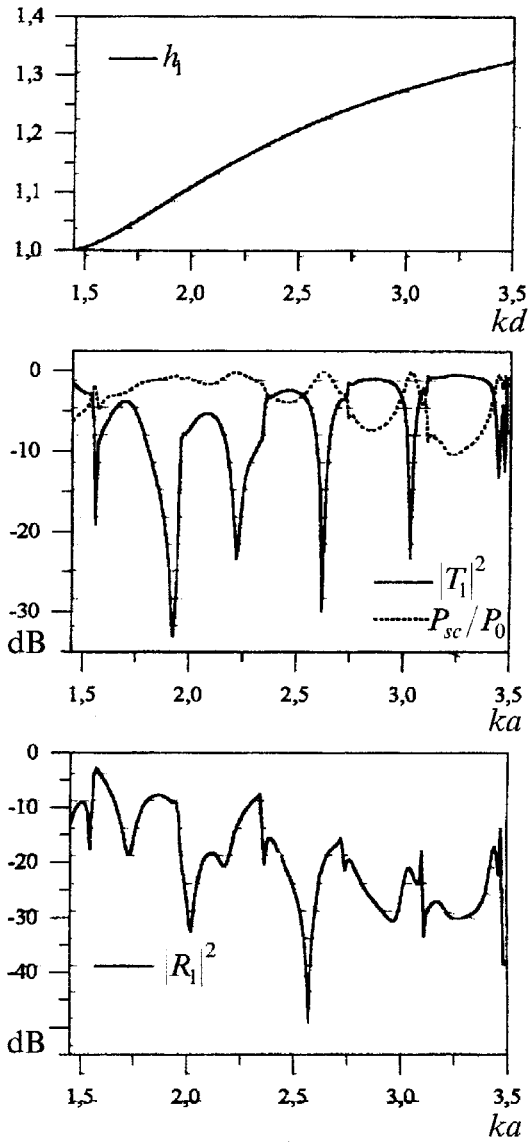

Fig. 4. *Far-field scattering characteristics versus ka for the dielectric resonator (E-polarization case).* ε_b*=10, w/a=0.01, d/a=1,* ε_s*=2.25*

At the resonances the filter characteristics were calculated versus the spacing. The results are plotted in Figs. 3 and 5c. In order to obtain an optimum performance the spacing between the waveguide and the resonator is to be selected properly.

As we consider an open structure it is necessary to study the radiation appearing when the dielectric slab mode is scattering from the resonator. The normalized radiation patterns are presented in Figs. 3 and 5a for dif-

ferent radii of the resonator. All plots in figures 3 and 5 correspond to resonances in Figs. 2 and 4.

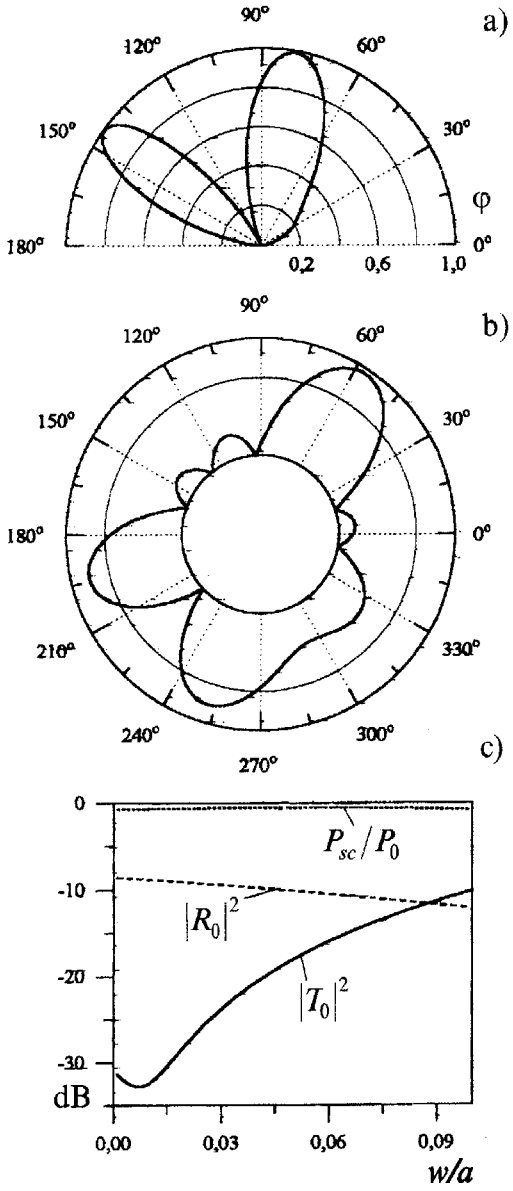

Fig. 5. *a) Normalized scattering pattern for the dielectric resonator (E-polarization case). ε_b=10, w/a=0.01, d/a=1, ε_s=2.25, ka=1.9242*
b) Electric field distribution on the contour of the resonator with the same parameters
c) Filter characteristics versus the spacing between the resonator and the waveguide

The dielectric cylinders show the advantages of WG-mode resonators, such as high quality factor and periodicity of stop bands. Due to these advantages, the filters on WG- mode resonators have undergone considerable development and are widely used in various microwave active and passive components. However there is an important feature, which seems to avoid recognition so far, probably due to a lack of correct analysis methods. Namely, at high-Q WG resonances the incident mode power is more than 99% converted to the radiation field.

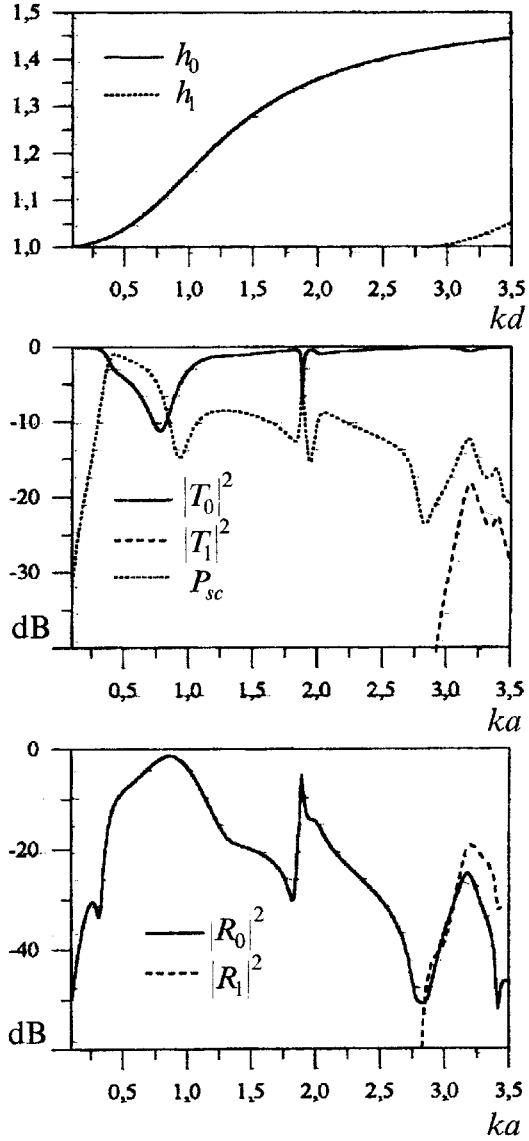

Fig. 6. *Frequency dependences of the far-field characteristics for the scattering from a metal cavity with parameters: θ=30°, φ_o=270°, w/a=0.01, d/a=1, ε_s=2.25*

Slitted metal cavity offers a way to avoid the excessive radiation and minimize the electric size of the filter. A resonance with a low level of radiation losses can be observed when the radius of the cylinder is smaller than the wavelength. In Fig. 6 the typical frequency dependences of transmitted ($P_T=|T|^2$), reflected ($P_R=|R|^2$), and scattered (P_{sc}) power fractions for the scattering from the metal slitted cavity are shown for the *H*-polarization case. When excited by the surface wave field, the cavity gives a resonant response provided that

the frequency coincides with the real part of a complex natural frequency of the slitted cavity. These eigenfrequencies are related to two families of modes, because of the splitting of the closed cylinder's doubly-degenerated modes, to symmetric and antisymmetric ones, by cutting a slot. It can be observed that antisymmetric resonances have a larger Q-factor then symmetric ones. The first low-frequency peak is due to the Helmholtz mode of a cavity-backed aperture (see [6,7]). The Helmholtz mode frequency is a complex number tending to zero when $\theta \to 0$. So, by narrowing the slot one can obtain a miniature low-frequency rejection filter with a remarkably low parasitic radiation: more than 90% of the incident mode power may be converted to the reflected mode. We did not consider the case of E-polarization because the most interesting low-frequency resonance does not exist.

4. Conclusions

We have proposed a full-wave approach to the analysis of surface-wave bandstop filters. Based on this approach the efficient numerical techniques were developed, and rejection, transmission and radiated-field characteristics were calculated for both E and H-polarizations.

Sharp resonant phenomena were observed for the scattering from dielectric cylinders and metal cavities. These effects can be used for the design of bandstop filters in surface-wave guides. Our investigations proved the advantages offered by such resonators that lead to their applications as microwave oscillators and filters. Unlike our previous study [8], in this paper we considered a waveguide with a multimode operation. Although in most practical situations a single mode operation is desired, it is interesting to analyze the effect of the newly-born mode on the filter characteristics. We emphasize that, due to the analytical regularization, our solutions are equally accurate off and near the sharp resonances, unlike the conventional MoM ones (see [12]). This fact makes them well suited to the computer-aided design of resonant microwave devices.

The presented numerical treatment deals with the surface wave scattering from obstacles, but the method is applicable to various types of incident fields (plane or cylindrical wave, etc.), and different host media.

Acknowledgment. The authors would like to express their thanks to Dr. A.G. Yarovoy for many helpful discussions, and to the SUMMA Foundation and IEEE MTT Society for support and encouragement.

References

1. N. Morita. IEE Proc. 1980, **27**, Pt. H., No. 5, pp. 263-269.
2. X.H. Jiao, P. Guillon, L. A. Bermudez and P. Auxemery. IEEE Trans. Microwave Theory Tech. 1987, **MTT-35**, No. 12, pp. 1169-1175.
3. Y. Filipov, S. Kharkovsky, A. Kirichenko. Micowave Opt. Technol. Lett. 1995, **10**, No. 2, pp. 124-129.
4. V.I. Kalinichev and P.N. Vadov. Soviet J. Commun. Technology and Electronics (English Transl.). 1988, **33**, No. 7, pp. 108-115.
5. N.K. Uzunoglu and J.G. Fikioris. J. Opt. Soc. Am. 1982, **72**, No. 5, pp. 628-637.
6. A.I. Nosich. Soviet Physics-Techn. Physics (Engl. Transl.). 1986, **31**, No. 8, pp. 883-889.
7. A.I. Nosich and A.S. Andrenko. IEEE Trans. Microwave Theory Tech. 1994, **MTT-42**, No. 2, pp. 298-307.
8. S.V. Boriskina and A.I. Nosich. Microwave and Opt. Technol. Lett. 1996, **13**, No. 3, pp. 169-173.
9. A.I. Nosich. J. Electromagnetic Waves Applic. 1994, **8**, No. 3, pp. 329-353.
10. A.G. Yarovoy. IEICE Trans. on Electronics (Japan). 1995, **E 78-C**, No. 10, pp. 1440-1446.
11. P.G. Petropoulos, G.A. Kriegsmann. IEEE Trans. Antennas Propagat. 1991, **AP-39**, No. 8, pp. 1119-1124.
12. G.L. Hower, R.G. Olsen, J.D. Earls and J.B. Schneider. IEEE Trans. Antennas Propagat. 1993, **AP-41**, No. 7, pp. 982-986.

Численный анализ фильтров поверхностных волн на диэлектрических резонаторах и полых металлических резонаторах с отверстиями связи

С. В. Борискина, А. И. Носич

Рассмотрена двумерная задача рассеяния поверхностной волны диэлектрического слоя на металлической подложке на диэлектрических цилиндрах кругового поперечного сечения и на металлическом полом резонаторе с отверстием связи. С использованием поверхностных потенциалов простого или двойного слоя с функциями Грина пространственно неоднородной среды и метода регуляризации разработаны эффективные численные алгоритмы и обсуждается применение таких рассеивателей в качестве полосно-заграждающих фильтров в волноводах поверхностных волн. Численно рассчитаны излученная мощность, и мощность, переносимая поверхностными волнами, а также сечения рассеяния в верхнее полупространство в точках резонанса. Проведено сравнение двух типов полосно-заграждающих фильтров.

Числовий аналіз фільтрів поверхневих хвиль на діелектричних резонаторах та порожнистих металевих резонаторах з отворами зв'язку

С. В. Борискіна, О. І. Носич

Розв'язано двовимірну задачу розсіяння поверхневої хвилі діелектричного шару на металевій підложці на діелектричних циліндрах кругового поперечного перерізу та на порожнистому металевому резонаторі з отвором зв'язку. Використовуючи метод поверхневих потенціалів простого або подвійного шару з функціями Гріна просторово-неоднорідного середовища та метод регуляризації, розроблено ефективні алгоритми та розглядається застосування таких резонаторів як смуго-загороджувальних фільтрів у хвилеводах поверхневих хвиль. Зроблено числові розрахунки випроміненої потужності та потужності, що переноситься поверхневими хвилями, а також діаграми розсіяння у точках резонансів. Проведено порівняння двох типів смуго-загороджувальних фільтрів.

(*) The field representation in terms of only the single-layer potential (6a),(6b) is not the most general one and leads to the appearance of the spurious (real-valued) eigenvalues of resulting IE. They spoil the algorithm because the IE condition number has poles at the spurious-eigenvalue frequencies. The severity of assocoated numerical error depends, however, on the details of the IE discretization scheme used. The full remedy is the use of the Muller IE which is completely equivalent to the original boundary-value problem and thus free of spurious eigenvalues.